Hydrol. Earth Syst. Sci., 26, 2637–2648, 2022
https://doi.org/10.5194/hess-26-2637-2022

Hydrology and Earth System Sciences
Open Access
EGU

$\delta^{13}C$, CO_2 / ^3He and ^3He / ^4He ratios reveal the presence of mantle gas in the CO_2-rich groundwaters of the Ardennes massif (Spa, Belgium)

Agathe Defourny[1,2], Pierre-Henri Blard[3,4], Laurent Zimmermann[3], Patrick Jobé[2], Arnaud Collignon[2], Frédéric Nguyen[1], and Alain Dassargues[1]

[1]Urban and Environmental Engineering, University of Liège, Liège, Belgium
[2]Water Resource Department, Spadel S.A., Spa, Belgium
[3]Centre de Recherches Pétrographiques et Géochimiques (CRPG), Université de Lorraine, CNRS, UMR7358, Nancy, France
[4]Laboratoire de Glaciologie, Université libre de Bruxelles (ULB), Brussels, Belgium

Correspondence: Agathe Defourny (adefourny@uliege.be)

Received: 3 December 2021 – Discussion started: 17 January 2022
Revised: 8 April 2022 – Accepted: 13 April 2022 – Published: 19 May 2022

Abstract. Although natural CO_2-rich groundwaters of eastern Belgium have been known for centuries, the exact origin of their gas is still unclear. This paper presents the results of a sampling campaign in Belgium (Spa, Stoumont, Malmedy): 30 samples of both carbogaseous and non-carbogaseous groundwaters were analyzed for major elements, CO_2 content and carbon isotopic composition. Among them, 13 samples were also analyzed for $^3He/^4He$ and $^4He/^{20}Ne$ ratios. The combination of $\delta^{13}C$ (between ca. -9 ‰ VPDB[1] and -2 ‰ VPDB), $CO_2/^3He$ ratio (between 1.9×10^8 and 2.9×10^9) and $^3He/^4He$ (between 0.92 and 2.70 Ra) shows with a high level of confidence that the CO_2 in the carbogaseous groundwater of Spa and Bru has a mantle origin. It can likely be attributed to the degassing of mantle from the neighboring Eifel volcanic fields, located at a distance of 100 km eastwards.

The identity and nature of the deep-rooted fractures that act as CO_2 transport pathways to the surface are still to be clarified, but several major thrust faults exist in the Rhenish Massif and could connect the Eifel volcanic fields with the studied area.

[1]Vienna Pee Dee Belemnite

1 Introduction

CO_2-rich groundwaters have always been a very fascinating geomanifestation, and their presence in a region is often the trigger of a strong economic and touristic activity. Lately, a better assessment of CO_2 circulation modes in the subsurface has gained interest, as it is important to finely document their contribution to the natural budget of atmospheric CO_2. Understanding the saturation state of CO_2 in groundwaters and in geological reservoirs is also important for CO_2 storage projects. Moreover, in areas where CO_2-rich groundwater is bottled as mineral water, it is essential to have a complete understanding of the whole system, to ensure sustainable exploitation of the resource. The presence of CO_2 in groundwater – in excess compared to the atmospheric equilibrium – can result from different phenomena, with the most common ones being a direct contribution from the mantle, the dissolution of carbonate rocks or an organic origin (Agnew, 2018). The discharge of CO_2 from deep geological structures to the surface is always the result of a specific geological context which involves a source of CO_2 at depth and an intricate system of faults acting as transport pathways to the local groundwaters, which is considered the final receptor.

This study focuses on the dozens of CO_2-rich groundwater springs that exist in the Ardennes massif in eastern Belgium. The most famous ones are located in the small city of Spa, whose springs have been known since the Roman Empire.

The name of the town became famous thanks to the development of thermalism in the 19th century and is now used worldwide to refer to wellness and bathing activities. These groundwaters yield natural springs at the surface, but they are also exploited as mineral water from boreholes. Their CO_2 content ($2 \pm 0.5\,g\,L^{-1}$) makes them slightly acidic (pH around 5.7). They have a high content of iron ($17 \pm 10\,mg\,L^{-1}$ on average but up to $50\,mg\,L^{-1}$). They, however, bear a relatively low TDS (total dissolved solid) value with a dry residue ranging between 80 and $160\,mg\,L^{-1}$ in comparison with other naturally sparkling mineral waters bottled in other European geological contexts (e.g., $940\,mg\,L^{-1}$ for San Pellegrino, $1100\,mg\,L^{-1}$ for Badoit, $3325\,mg\,L^{-1}$ for Vichy Célestins, as stated on bottle labels).

Although these springs have been bottled for centuries and studied for many years, the origin of their high CO_2 content has not been established already. Helium isotopes, elemental $^4He/^{20}Ne$ and CO_2 isotopic composition of dissolved gas are powerful tools to identify the sources of these gas (Sano and Marty, 1995; Karolyte et al., 2019; Gilfillan et al., 2019). In this paper, we present the ^3He, ^4He, ^{20}Ne and CO_2 concentrations measured in 13 groundwater samples of the Spa and Bru areas (Ardennes, Belgium), together with hydrochemical analysis on major elements for 30 samples, to identify the origin of dissolved CO_2 in groundwater and to explore the potential hydro-connection with the Eifel volcanic fields (western Germany), where similar CO_2-rich groundwaters are found.

2 Geological context

2.1 Regional geology

CO_2-rich mineral waters from eastern Belgium are located in the Rhenish Massif, which is part of the Rhenohercynian fold belt (Vanbrabant et al., 2002). This massif extends through western Germany, eastern Belgium, Luxembourg, and a part of France, as shown in Fig. 1. The Rhenish Massif is dominated by Paleozoic rocks and is separated into two parts by the Rhine Graben. The western part, the Ardennes (eastern Belgium), is bordered to the north by the Midi-Eifel thrust fault. In the Ardennes region, the Rhenish Massif is dominated by the Ardennes Allochthon, consisting of a Cambro-Ordovician basement unconformably overlain by Devono-Carboniferous sandstones and limestones (Barros et al., 2021) (Fig. 1).

The present regional geology is the result of several stages. The oldest rocks that can be observed in Belgium are found in the Ardennes region; they consist of Cambrian to Ordovician sediments deposited in deep-platform marine environments. They mainly consist of fine clays in alternation with sandstones. During the Late Silurian, the Caledonian orogeny faulted and folded these layers and induced a strong metamorphism. Compression and shearing of claystone produced a well-expressed schistosity, while sandstone evolved into quartzites. The metasediments observed today are therefore an alternation of clays and sandstones metamorphosed into slates ("phyllades") and quartzites, which are called "quartzophyllades" in the region. Then, after an emersion and erosion period, sedimentary deposition started again during the Lower Devonian, in unconformity over the folded rocks. During the Lower Devonian period, limestones were deposited in vast carbonate platforms. Then, sandstones accumulated in coastal detrital environments during the Devonian.

At the end of the Devonian, the Variscan orogeny took place, inducing another phase of tectonic deformation. During this orogeny, the Dinant Synclinorium and the Ardennes massif were displaced several kilometers northward. This (latter) unit constitutes the Ardennes Allochthon, a great anticlinal ensemble that is limited to the north by the Midi-Eifel thrust fault. Three Cambrian massifs are identified within the Ardennes Allochthon: the Rocroi, the Givonne and the Stavelot massifs. The studied springs are located within the Stavelot Massif and at its border with the Dinant Synclinorium. The Malmedy Graben, filled with Permian conglomerates, developed in the center of the Stavelot Massif with an SW–NE orientation is separating the Stavelot Massif into two parts (Barros et al., 2021).

2.2 CO_2-rich groundwater springs in the Rhenish Massif and the Eifel volcanic fields

Numerous occurrences of CO_2-rich groundwater springs are recorded in the Rhenish Massif, as shown in Fig. 2. CO_2-rich groundwaters that are present in Belgium are cold waters (12 °C on average). They are fed by the recharge from local or regional precipitation, as confirmed by ^{18}O and ^2H isotopic measurements (Barros et al., 2021). The system is dominated by metamorphized sedimentary rocks, and the aquifer zones lie in the first hundreds of meters of these deposits, in the fractured and weathered parts.

Naturally sparkling groundwaters are bottled by three different companies in the area (Bru-Chevron and Spa Monopole in Belgium and Gerolsteiner Brunnen in Germany). While it has been proven several years ago that the dissolved CO_2 present in the springs of western Germany was the result of mantle degassing, this was not confirmed for the Belgian springs yet (May et al., 1996; Aeschbach-Hertig et al., 1996; Barros et al., 2021).

However, the proximity between the two gas-rich groundwater areas, their common geological context and the scale of the Eifel volcanism suggest that the gas they contain might have a common origin. In the Eifel area, volcanic activity has occurred during the Quaternary. It is thought that the lower-mantle upwelling under central Europe may feed smaller upper-mantle plumes (Goes et al., 1999). Indeed, small plume structures have been identified below the Eifel area by teleseismic tomography (see Ritter et al., 2001), and

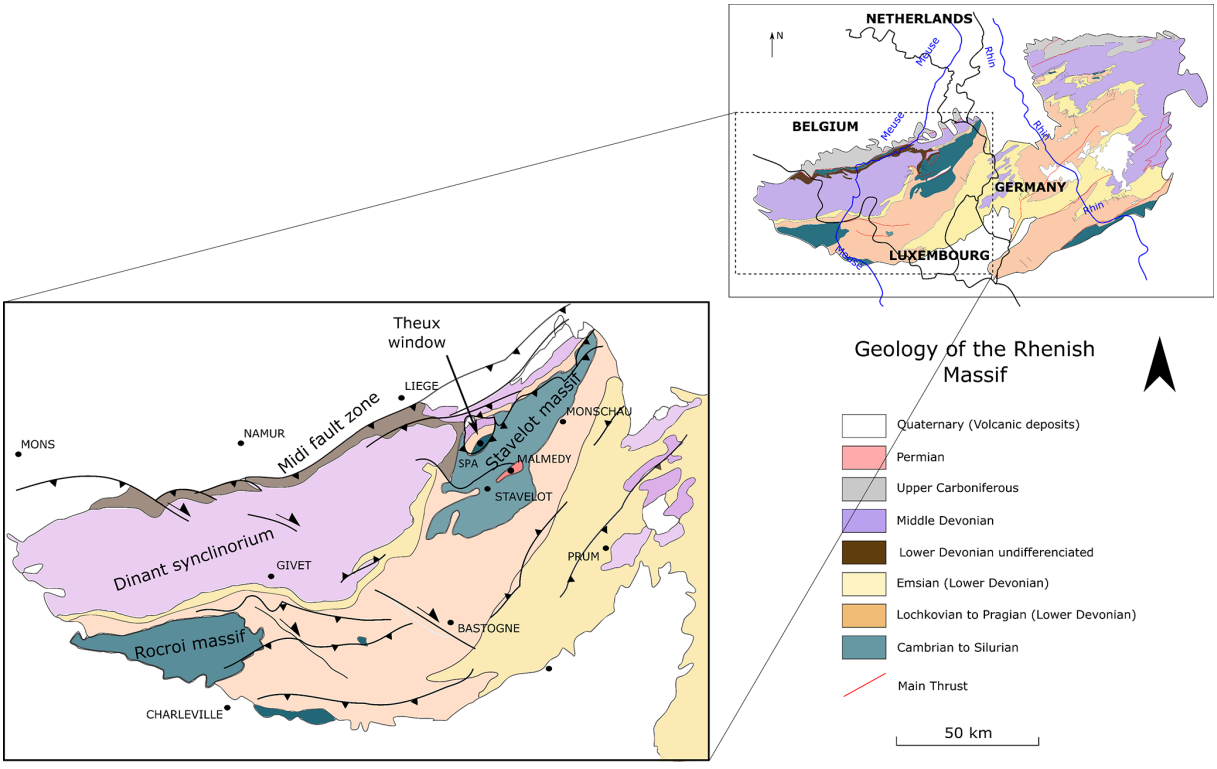

Figure 1. Simplified geology of the Ardennes Allochthon and its localization in western Europe and in the Rhenish Massif, modified after Fielitz and Mansy (1999).

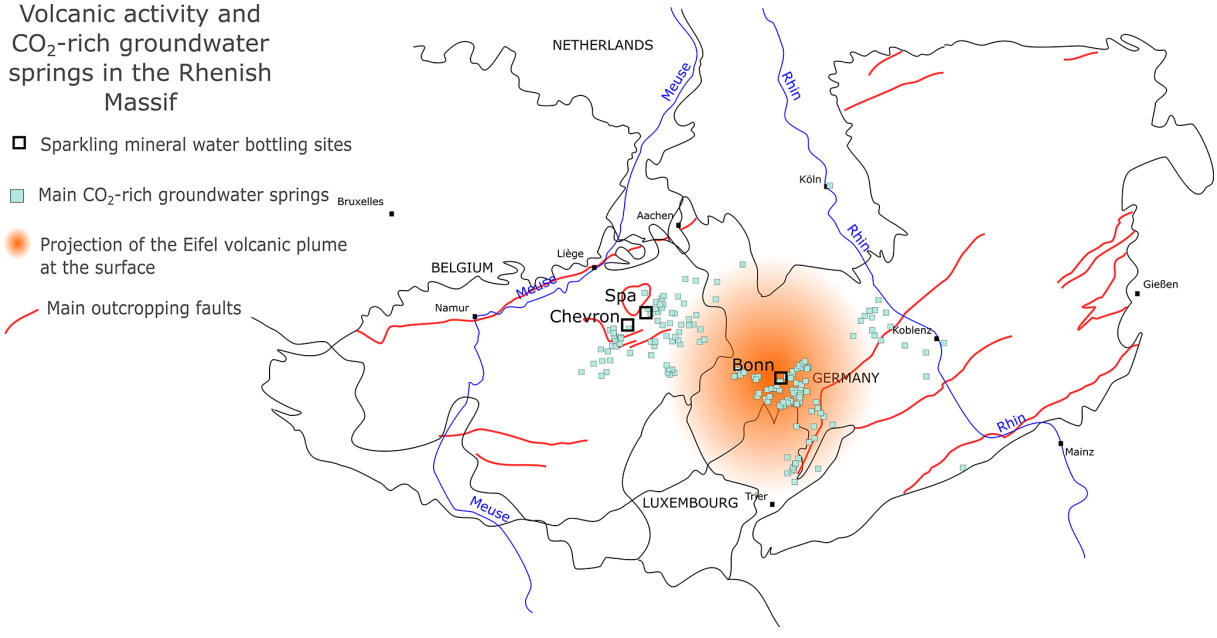

Figure 2. Occurrences of CO_2-rich groundwater springs in the Rhenish Massif, together with the main bottling sites. The spring locations were compiled from May et al. (1996), Bräur et al. (2013) and internal data from Spadel. The projection of the Eifel volcanic area is depicted after Bräur et al. (2013).

a recent study by Kreemer et al. (2020) has shown that this plume was still buoyant (Kreemer et al., 2020). However, recent studies on the isotopic composition of noble gas in the Eifel area and in Massif Central (France) tend to confirm a direct contribution from the upper mantle (mid-ocean-ridge basalt, MORB). The exact origin of the Eifel volcanism is thus still a matter of debate (Bekaert et al., 2019; Moreira et al., 2018).

3 Sampling and analysis

For this study, water samples from both natural springs and wells were collected at 30 different locations distributed within an area (30 km × 20 km) belonging to the Spa, Bru or Malmedy regions (Table 1, Fig. 3). Each of them has been analyzed for major and trace elements, physicochemical parameters, dissolved gases (O_2, CO_2, He, Ne), and carbon isotopes ($\delta^{13}C$). During a second campaign, 13 of these 30 sites were resampled, with the specific purpose of analyzing their $^3He/^4He$ and $^4He/^{20}Ne$ isotopic ratios. Samples were stored in copper tubes clamped on both sides to prevent any degassing or air contamination.

Major and trace elements, together with physicochemical parameters and dissolved O_2 and CO_2, were measured at the Spadel hydrochemistry laboratory, following the specific certified procedures: ISO 10523 (pH), ISO 7888 (electrical conductivity), ISO 10304-1 (chlorides, sulfates and nitrates), ISO 9963 (bicarbonates), ISO 17289 (dissolved oxygen) and ISO 17294 (ICP-MS[2] for the rest of the elements). Dissolved CO_2 was quantified by mineral sequestration via a barium sulfate saturated solution, followed by an inverse titration. Carbon isotopic ratios were measured by a private lab using isotope-ratio mass spectrometry (IRMS) and gas chromatography isotope-ratio mass spectrometry (GC-IRMS). Finally, the dissolved concentrations of helium isotopes were analyzed at the CRPG of Nancy (CNRS-UMR 7358) by static vacuum mass spectrometry after vacuum extraction and purification according to Zimmermann and Bekaert (2020) and Zimmermann et al. (2015). The $^4He/^{20}Ne$ ratio was also measured in the same water aliquots, with a quadrupole installed on the extraction line. Instrument sensitivity was determined against a gas standard having an atmospheric composition. Tap water that had been placed in equilibrium with the atmosphere was also analyzed for comparison (Table 1).

Figure 3 shows the location of each sample in the local geology.

4 Results

Table 1 presents the gas results measured in our 30 new samples. Data from Victoriaquelle (VQ) and Schwefelquelle (SQ) are from Marty et al. (2020). Data from the Laacher See Mofetta (LaS) and Wehr 10 well (W10) (Bräur et al., 2013) are also included (i.e., a *mofetta* is a fumarole discharging mostly carbon dioxide). All these values can be compared to the mid-ocean-ridge basalt (MORB) endmember, which is commonly accepted to represent the signature of the upper mantle and has been studied in detail by Graham (2002).

All the data obtained from these groundwater samples of Spa, Bru and Malmedy (cations, anions, dissolved CO_2, $^3He/^4He$ and $^4He/^{20}Ne$ ratios) are available in Table 1.

5 Discussion

5.1 Chemical composition of groundwater and dissolved gases

The Piper diagram presented in Fig. 4 shows the relative proportion of cations and anions for each sample. The figure shows a calcium–magnesium–bicarbonate type for most samples. Regarding the cations (Ca, Mg, Na + K), the majority of the samples have rather closed compositions and display a globally balanced composition, with the less abundant cation representing in any case at least 10 % of the total. CGB samples are composed of a smaller proportion of Na + K with a bigger proportion of Mg compared to CGS samples. One exception to this balanced composition in cations is the *PdI* sample, which is computed on a near-pure calcium pole, probably because it was sampled in a zone influenced by the carbonate-rich conglomerate of the Malmedy Graben (shown in Fig. 3). The distinction between CG and NCG groundwater samples is much clearer looking for their anion compositions. There is a significant relative enrichment of CG samples in bicarbonates, due to the presence of dissolved CO_2. Only the samples *Art* and *PlG* are out of the range of this carbonate-rich cluster. However, this lower carbonate content is only relative as the sample *Art* has a much higher concentration in sulfates (16.7 mg L^{-1}, whereas most samples contain < 5 mg L^{-1}), presumably from a local geological origin, and the sample *PlG* has a higher chloride content (58.2 mg L^{-1}, whereas the average composition of the other samples is around 5 mg L^{-1}). The latter is presumably from an anthropic origin.

This figure indicates that both CO_2-rich and non-CO_2-rich groundwaters have initially similar compositions, mainly driven by the local lithologies. The enrichment of CO_2 and bicarbonates in groundwater leads to an acidification of groundwater. Hence, CO_2-rich groundwaters are generally more corrosive and more mineralized. However, the waters of this dataset keep the same relative proportions in cation composition, whatever their carbonate contents (Fig. 4). This observation is not really in line with the hypothesis that carbonate dissolution explains the main origin of this dissolved CO_2. As discussed in Barros et al. (2021), this hypothesis was until now the most commonly accepted one for the CO_2 origin. Indeed, if the presence of dissolved CO_2 in carbo-

[2]Inductively coupled plasma mass spectrometry

Table 1. Analysis results for the 30 samples. CGB = carbogaseous water from the Bru area, CGS = carbogaseous water from the Spa area, NCGB = non-carbogaseous water from the Bru area, NCGS = non-carbogaseous water the from Spa area, and CGM = carbogaseous water from the Malmedy area. R / R_a is the He isotopic ratio expressed with regard to the ratio in air. VPDB is the Vienna Pee Dee Belemnite standard, reporting the abundance of carbon. DIC stands for dissolved inorganic carbon.

	Type		pH	CE	Ca	Mg	Na	K	Cl	SiO_2	HCO_3	SO_4	Fe	Mn	CO_2	O_2	$\delta^{13}C$ DIC ±0.3 ‰	R / Ra	±	$^4He/^{20}Ne$	±
				µS cm^{-1}	mg L^{-1}	mg L^{-1}	mg L^{-1}	mg L^{-1}	mg L^{-1}	mg L^{-1}	mg L^{-1}	mg L^{-1}	mg L^{-1}	mg L^{-1}	g L^{-1}	mg L^{-1}	‰ VPDB	–	–	–	–
BdB	CGB	Well	5.2	301	21	15.63	6.92	1.67	3.3	20.84	143	<5	16.19	1.39	2.68	2.47	−2.4	2.7	0.02	150.63	9.55
Moi	CGB	Spring	5.4	424	25.7	24.93	8.51	1.71	4.2	17.58	234	<5	25.15	1.86	1.81	2.89	−2.9				
Mon	CGB	Well	5.6	556	68.4	23.24	13.1	1.75	5	21.24	315	<5	7.05	1.3	2.02	2.86	−3.4	2.42	0.02	154.35	5.4
SB	CGB	Spring	5.1	232	12.3	11.43	7.46	0.97	3.9	20.98	91	<5	13.93	1.14	2.15	3.58	−3.4				
Abb	CGB	Well	5.9	274	23.4	12.91	8.7	0.78	4	30.9	152	7.5	6.77	1.36	0.7	9.49	−8.8	2.61	0.02	68.16	2.7
PdM	CGB	Well	5.9	223	23.9	10.76	5.65	1.07	12.8	7.07	100	<5	7.46	0.48	0.77	6.95	−8.7	2.42	0.01	33.19	1.54
PS	CGB	Well	5.3	454	23.7	24.1	4.67	1.5	3.4	17.7	231	<5	35	2.11	3.45	0.33	−2.4	2.5	0.01	348.68	16.6
Art	CGS	Well	5.3	100	4.3	3.39	4.01	0.42	5.4	7.2	23	16.7	5.46	0.13	0.91	5.58	−7.6	1.15	0.01	69.64	2.12
CG4	CGS	Well	5.8	212	16.7	9.29	8.35	1.46	4.5	7.5	113	<5	7.14	0.24	1.22	6.71	−5.7				
PlP	CGS	Well	5.4	257	15.9	9.32	4.97	0.84	3.1	10.04	137	<5	22.06	0.38	2.35	0.76	−3.8				
PlF	CGS	Well	5.8	312	30.4	10.16	20.46	6.48	3.6	11.25	169	11.8	4.04	0.16	1.27	2.46	−4.9	1.85	0.02	45.19	1.65
HF	NCGB	Well	6.5	168	15	3.76	12.04	0.83	5.3	16.58	63	17	0.26	0.53	0.14	8.11	−15.7	1.87	0.01	4.05	0.16
FH	NCGB	Well	6.5	169	21.2	2.69	7.67	1	4.1	14	64	16.1	0.098	0.43	0.01	9.57	−15.2	1.73	0.01	1.66	0.07
AuE	NCGS	Well	5.8	52	3.8	1.98	2.27	0.2	3.1	7.05	12	7.8	2.07	0.05	0.09	2.52	−22.6	1.65	0.01	2.66	0.12
F9	NCGS	Well	5.8	38	3.3	0.78	2.46	0.26	3.2	7.13	8	<5	0.85	0.02	0.02	4.06	−27.0				
Sop	NCGS	Well	6.4	92	8.4	2.05	6.26	0.49	5.2	13.57	32	5.7	<0.005	0.005	0.12	6.13	−18.3	1.06	0.02	4.79	0.24
Mey	NCGS	Well	6	64	4.3	1.8	2.68	0.28	3.6	6.77	19	7.8	2.29	0.05		5.72	−17.6				
PlG	CGS	Spring	5.7	809	42.7	35.47	71.52	4.75	58.2	54.56	>204	12.8	17.35	1.81	2.64	0.56	−4.5				
Ton	CGS	Spring	5.1	195	11.9	7.24	6.57	0.79	10.7	16.73	71	<5	13.33	0.92	2.24	0.84	−3.9				
Bar	CGS	Spring	5.3	239	12.1	9.77	17.36	1.16	5.6	27.22	114	<5	9.95	1.2	2.10	0.77	−4.2	1.1	0.02	106.93	3.12
Ger	CGS	Spring	5.7	185	15.3	7.55	9.74	1.23	5.9	11.61	92	<5	4.15	0.19	1.28	3.63	−5.9				
Sau	CGS	Spring	5.5	336	27.9	13.38	12.26	1.33	5.5	10.04	182	<5	31.95	0.7	2.14	2.3	−3.9				
Del	CGS	Spring	5.6	298	22.7	14.15	16.03	2.12	3.5	10.94	170	<5	6.54	0.17	1.39	3.61	−4.7	0.92	0.01	278.02	11.42
TdB	CGB	Spring	5.9	856	108.8	46.28	20.12	1.8	4.4	20.12	539	<5	51.91	2.76	3.12	0.27	−2.1				
Vic	CGB	Spring	5.2	287	19.5	13.76	7.84	1.19	3.8	23.36	131	<5	37.52	2.72	2.08	1.26	−2.9				
Ern	CGB	Spring	5.8	863	46.6	30.3	104.49	5.09	59.6	9.77	414	<5	8.34	0.76	2.32	1.82	−2.9				
Bern	CGM	Spring	5.4	167	10.3	6.24	3.21	0.52	5.8	8.13	66	<5	13.14	0.47	1.3	3.92	−4.0				
PdI	CGM	Spring	6.3	2440	418.6	<0.4	68.71	5.78	37.8	12.61	1736	14.6	29.3	6.26	2.89	1.03	−1.8				
Berl	CGB	Spring	6.3	323	28.2	8.56	7.16	1.2	14.2	8.8	165	5.2	25.49	2.1	0.95	5.49	−3.4				
Har	CGB	Spring	5.8	672	38.4	37.2	45.02	2.88	26.6	33.3	366	<5	14.86	0.73	2.49	2.54	−2.9				
VQ	CGE	Spring															−2.1	4.4		1880	
SQ	CGE	Spring															−2.0	4.5		1520	
LaS	Gas	Mofette																5.4		38	
W10	CGE	Well																5.6		1380	
MORB																		8.1		1000	
Tap																		0.971	0.052	0.292	0.013

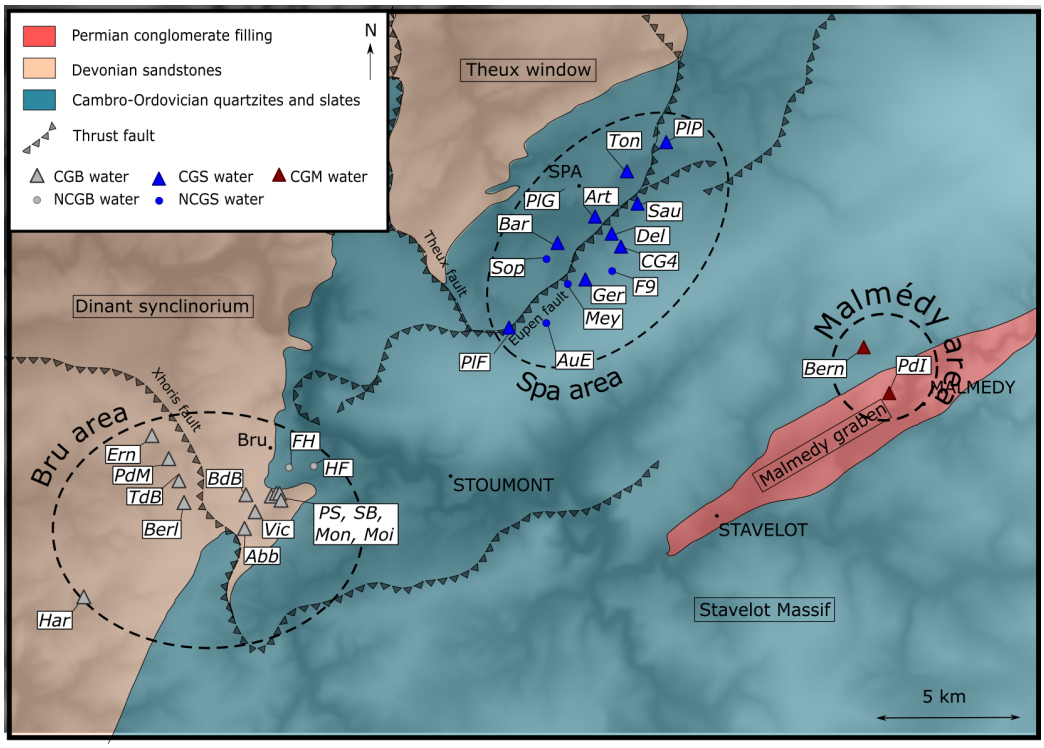

Figure 3. Location of each sample with regard to the main geological features.

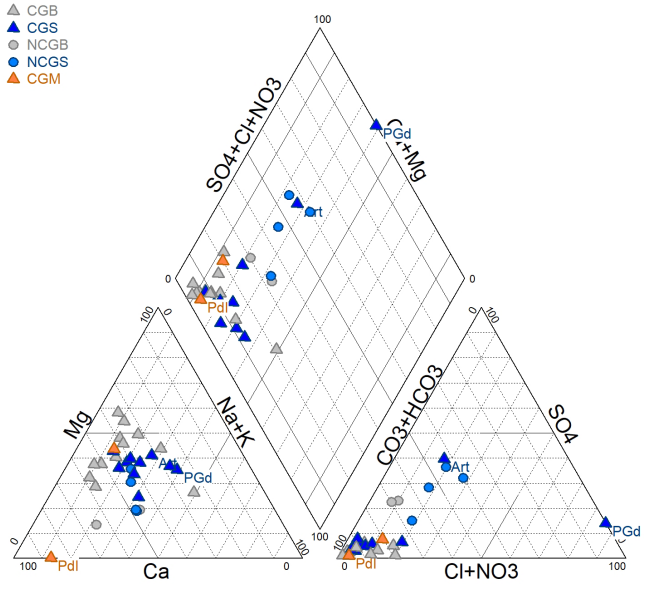

Figure 4. Piper diagram representing the relative proportion of cations and anions for each sample. CGB = carbogaseous water from the Bru area, CGS = carbogaseous water from the Spa area, NCGB = non-carbogaseous water from the Bru area, NCGS = non-carbogaseous water from the Spa area, and CGM = carbogaseous water from the Malmedy area.

gaseous waters was due to carbonate dissolution, it would be expected that this groundwater would also be enriched in Ca^{2+} and possibly Mg^{2+} ions in comparison to non-carbogaseous waters, but this is not the case in these Spa–Bru waters.

5.2 Constraining gas origin with helium and carbon isotopes

Inorganic carbon isotopes have proven to be a very powerful tool to make the distinction between different carbon sources. This isotopic proxy is particularly adapted to sparkling mineral waters (Fillimonova et al., 2020; Carreira et al., 2014; Redondo and Yelamos, 2004). However, the contribution of each carbon source is sometimes difficult to deconvolve. For example, a bulk C composition resulting from the mixing between marine limestones ($\delta^{13}C \approx 0\,‰$) and organic sediments ($\delta^{13}C \approx -20\,‰$) may have a $\delta^{13}C$ similar to that of mid-ocean-ridge basalt (MORB) ($\delta^{13}C \approx -6.5 \pm 2.5\,‰$), as shown by Sano and Marty (1995). Atmospheric $\delta^{13}C$ is estimated to be around $-8\,‰$ (Karolyte et al., 2019).

The $\delta^{13}C$ values of inorganic carbon measured in our samples range between $-8.8\,‰$ VPDB and $-1.8\,‰$ VPDB for CG groundwater samples and between $-27\,‰$ VPDB and $-15.2\,‰$ VPDB for NCG groundwater samples. The distinction between CG and NCG groundwaters is clear: NCG groundwaters have much lighter carbon isotopic ratios. The majority of $\delta^{13}C$ values in CO_2-rich groundwater are clus-

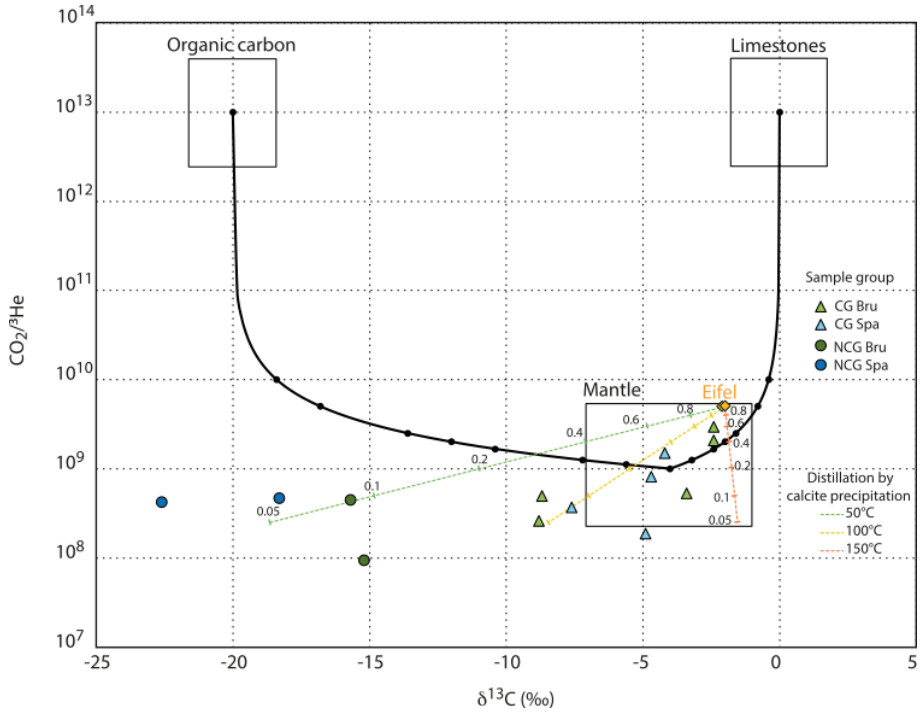

Figure 5. $CO_2/^3He$ ratios vs. $\delta^{13}C$ values for groundwater samples in relation to mixing between the mantle, carbonate and organic CO_2 endmembers based on Sano and Marty (1995). CGB = carbogaseous water from the Bru area, CGS = carbogaseous water from the Spa area, CGE = carbogaseous water from the Eifel area, NCGB = non-carbogaseous water from the Bru area, and NCGS = non-carbogaseous water from the Spa area. Gas Eifel composition from Marty et al. (2020). *VQ*, *SQ* and MORB are depicted from the values presented in Marty et al. (2020). All CO_2-rich groundwater samples fall in or close to the mantle range. Non-CO_2-rich groundwater samples present much lighter C isotopic composition. The impact of calcite precipitation at three temperature (50, 100 and 150 °C) is modeled assuming an open system Rayleigh distillation, following Ray (2009) and Barry et al. (2020).

tered around the mantle endmember, but some of them may also be compatible with a limestone origin (Fig. 5).

The combination of $\delta^{13}C$ with the $CO_2/^3He$ ratio permits us to make the distinction between the three main sources of dissolved carbon (mantle, limestone, organic carbon; Sano and Marty, 1995), as shown in Fig. 5: with the production of ^3He in the crust being negligible (Andrews and Kay, 1982), a high ^3He content (and hence a low $CO_2/^3He$ ratio) is the signature of a mantle carbon input. It can be observed in Fig. 5 that CO_2-rich groundwater samples have $CO_2/^3He$ and $\delta^{13}C$ values that are compatible with (or very close to) the mantle MORB endmember. These compositions are quite close to those of the volcanic gas of the Eifel area (Marty et al., 2020) (*SQ, VQ* samples). Although the Spa–Bru CG groundwaters have $\delta^{13}C$ values quite close to a limestone source, their $CO_2/^3He$ ratio is 2 to 4 orders of magnitude lower than the limestone endmember. Their clear enrichment in ^3He demonstrates that the gas dissolved in the Spa–Bru groundwaters has a mantle origin, probably from the nearby Eifel volcanic fields.

Although most of the CG waters are close to the mantle endmember in this $CO_2/^3He$ vs. $\delta^{13}C$ signature, some data points do not perfectly match the mixing lines between the three endmembers. Other processes that may have fractionated the initial $CO_2/^3He$ and $\delta^{13}C$ signatures thus need to be considered (e.g., Ray, 2009; Barry et al., 2020). With CO_2 and helium having different solubilities, partial degassing may fractionate the $CO_2/^3He$ ratio. However, with the solubility of CO_2 being larger than the one of helium, this process should lead to an increase in the $CO_2/^3He$ ratio of waters affected by degassing ratio, which is contrary to what we observe here. Moreover, there is almost no correlation between the $CO_2/^3He$ ratios and the dissolved helium concentrations (after correction for atmospheric helium), which is an observation that makes this process unlikely (Table 1). Another physical process that has the ability to modify the initial $CO_2/^3He$-$\delta^{13}C$ signature is the precipitation of calcite, leading to lower the $\delta^{13}C$ and the $CO_2/^3He$ by a Rayleigh distillation (in open system). In Fig. 5, following Ray (2009) and Barry et al. (2020), we modeled the effect of calcite precipitation at various temperatures (50, 100 and 150 °C), assuming an initial gas composition similar to the Eifel endmember (Marty et al., 2020). Although this process may, in theory, explain part of the scatter observed within the carbogaseous sources of Spa and Bru, we should, however, be cautious, because calcite precipitation has never been observed

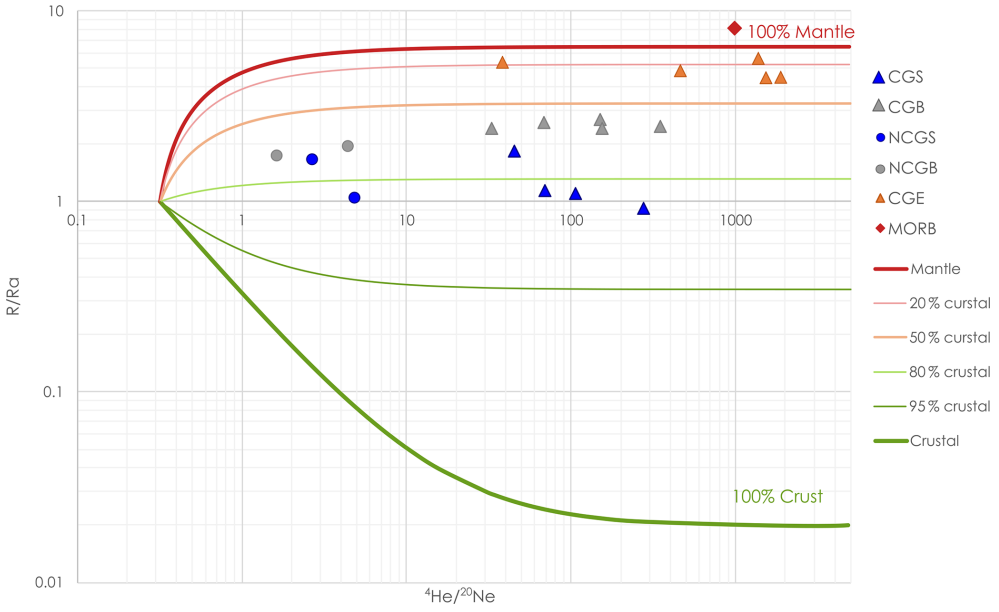

Figure 6. Proportion of crustal and mantle He in the samples, based on R / Ra and $^4He/^{20}Ne$ values. CGB = carbogaseous water from the Bru area, CGS = carbogaseous water from the Spa area, CGE = carbogaseous water from the Eifel area, NCGB = non-carbogaseous water from the Bru area, and NCGS = non-carbogaseous water from the Spa area. Mixing lines are computed from Eqs. (3) and (2). Values from Eifel and MORB are depicted from Marty et al. (2020). He atmospheric contribution is negligible. He crustal contribution appears to be more important for CG samples from the Spa area, as the local lithology is richer in uranium minerals.

in any of the many boreholes that have been installed in the area for water production, i.e., in the underlying rocks where these fluids are supposed to have transited. It is nevertheless important to stress that this fractionation does not hamper the identification of a clear mantle signature.

The low $\delta^{13}C$ and $CO_2/^3He$ values of the non-carbogaseous sources stand below the pure mixing curve between the mantle and organic carbon endmembers (Fig. 5). Our geochemical dataset (Table 1) shows that these gas-poor fluids are non-carbogaseous groundwaters that have never been enriched with gas, explaining their very different composition and depletion of $\delta^{13}C$ and CO_2.

5.3 Discriminating He origin with He and Ne isotopes

He isotopic ratios are normalized against the atmospheric isotopic composition and are expressed in R_a (considering atmospheric $^3He/^4He = R_a = 1.382 \times 10^{-6}$ (Sano and Fischer, 2013)). In these waters, R_a ranges between 0.92 and 2.70 (±0.02). $^4He/^{20}Ne$ ratios are very variable with values ranging from 1.7 to 348.7 (±4 %). Based on the measured $^4He/^{20}Ne$ ratios and assuming all ^{20}Ne of atmospheric origin, the contribution of atmospheric He can be computed using mixing Eq. (1), where $^4He/^{20}Ne_{air}$ is considered equal to 0.267 according to Holocher et al. (2001), and $^4He/^{20}Ne_{mantle}$ is equal to 1000 according to Dunai and Baur (1995).

$$\%He_{atm} = \frac{1 - \frac{^4He/^{20}Ne_{mantle}}{^4He/^{20}Ne_{sample}}}{1 - \frac{^4He/^{20}Ne_{mantle}}{^4He/^{20}Ne_{air}}} \quad (1)$$

This shows that atmospheric helium is negligible for all CG samples (less than 0.5 %) but more important for NCG samples (between 5 % and 15 %). The measured $^3He/^4He$ ratios allow for the computation of the origin of helium, which appears to be a mixture of crustal and mantle helium. The proportion of each source (crust and mantle) may be computed according to mixing Eqs. (2) and (3), where $^3He/^4He_{crust}$ and $^3He/^4He_{mantle}$ are taken to be equal to 0.02 and 6.5 Ra, respectively, according to Dunai and Baur (1995). We chose this 6.5 Ra "mantle" endmember as representative of the subcontinental lithospheric mantle (Dunai and Baur, 1995).

$$\%He_{mantle} = \frac{(1 - \%He_{atm})(^3He/^4He_{crust} - ^3He/^4He_{sample})}{^3He/^4He_{crust} - ^3He/^4He_{mantle}}, \quad (2)$$

$$\%He_{crust} = 1 - \%He_{mantle}. \quad (3)$$

Crust–mantle mixing lines are also displayed in Fig. 6.

Helium present in groundwater samples appears to be between 50 % and 80 % from crustal origin. A distinction can

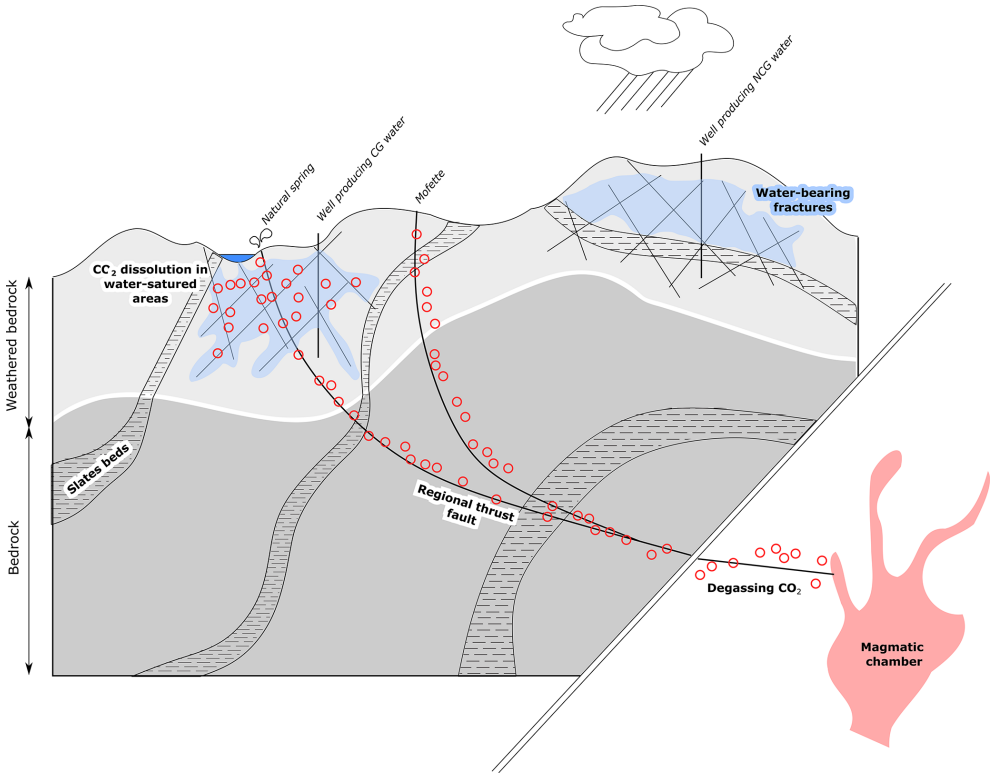

Figure 7. Updated conceptual model for the existence of CG and NCG groundwaters. Aquifer zones are located in the weathered parts of the bedrock. The aquifer in fractured, and slate beds isolate aquifer zones from each other. Degassing CO_2 from the mantle is brought to the system through regional thrust faults, and dissolved in groundwater.

be made between CG samples from Spa and Bru area, samples from Spa displaying more crustal helium (from 66 % to 81 %) than those of Bru (ranging from 54 % to 57 %). This may result from the local lithologies: Cambrian and Ordovician rocks from the Stavelot Massif are known for their high uranium content, often leading to high radon concentrations in cellars and underground buildings and also ^4He production through alpha decay (Depret et al., 2021; Vanderschueren, 2011). CG samples of Spa also differ from Eifel samples since they bear a larger proportion of crustal helium than the groundwaters of this volcanic region, where more than 80 % of He is from the mantle.

5.4 Conceptual model of groundwater and gas circulation

$CO_2/^3He$ and $\delta^{13}C$ measured in the samples from eastern Belgian springs show that the dissolved CO_2 present in the springs from eastern Belgium originates from a mantle contribution. The similar cation proportions for both CG and NCG groundwaters support the hypothesis that both groundwater types are initially the same (i.e., having the same origin). This is at odds with the commonly accepted hypothesis according to which CG groundwater would travel at several kilometers depth to meet and dissolve carbonated layers, where it could have acquired its dissolved CO_2 content before flowing upward rapidly to the surface. This hypothesis is also whittled by the fact that CG groundwaters are cold groundwaters, having similar temperatures to NCG groundwaters (between 12 and 13 °C). Assuming a vertical temperature gradient of 30 °C km^{-1}, this suggests that water circulation does not occur deeper than a few hundred meters below the surface. $^3He/^4He$ ratios indicate that crustal ^4He enrichment occurred during the water circulation in the aquifer, but such addition of crustal fluid is impossible in less than 1 km flow water paths.

The conceptual circulation model of water and gas at depth has then to be updated and is shown in Fig. 7. The conceptual model is very similar to one of the models described by Pisolkar (2017) in his work aiming at developing integrated hydrogeological models representing the classical properties of CO_2-rich mineral water systems in different contexts.

Considering all our data with those by Barros et al. (2021) (notably the isotopic $\delta^{18}O$ and D / H composition of the water), we propose here a revised model (Fig. 7) to explain the origin of the gas-rich groundwaters of the Spa–Bru massif, involving the input of CO_2-^3He-rich gas from the nearby Eifel massif through deep crustal faults.

The geomorphology of the system is mostly controlled by basin structures and anticlines. Slate beds act as low per-

meability barriers partitioning the aquifer and isolating the different compartments. Small faults and surface weathering enable the infiltration and storage of water from the surface to the underground, whereas major deep-rooted faults act as CO_2 transport pathway from degassing mantle that can be located several tens of kilometers away from the local aquifers. Where major faults reaching the surface do not encounter a sufficiently permeable and water-saturated zone (i.e., in the slates covered by a clayey colluvium as a result of weathering processes), CO_2-^{3}He-rich dry gases are discharged to the surface and mofettes are observed. The discharge points are mainly springs (at low topographic points or at geological low permeability/high permeability contacts) in the hillslopes or water abstraction wells.

The $CO_2/^3He$ and $\delta^{13}C$ composition of the samples is very close to samples taken in the Eifel volcanic fields (Fig. 5, Table 1); considering the proximity of the two sites (distance less than 100 km), it seems very likely that the gas found in the Belgian springs comes from the degassing of the mantle in the Eifel volcanic fields. In the future, the link between the two regions needs to be further explained in terms of structural geology.

The main structural features existing in the area are the Eupen thrust fault, the Xhoris thrust fault and the normal faults linked to the opening of the Malmedy Graben (see Fig. 1). All these faults could be connected at several kilometers depth to the Midi-Eifel thrust fault, which is a major thrust fault corresponding to the northernmost front of the Variscian orogeny and connecting both regions. This fault acts as an important seismic reflector and could thus be observed below the Stavelot Massif thanks to seismic measurement surveys lead by the DEKORP research group in the early 90s (Stiller et al., 1987).

The exact origin of the Eifel volcanism, between a plume or an upper-mantle contribution, is still a matter of debate. Unfortunately, although the results confirm the magmatic origin of the gas dissolved in groundwater, they do not provide new information to support one or the other hypothesis.

6 Conclusions and future research

This paper answers a long-standing question regarding the origin of the dissolved CO_2 in the naturally sparkling mineral waters of eastern Belgium. The combination of $\delta^{13}C$ and ^{3}He isotopes have shown with a high level of confidence that the dissolved CO_2 in groundwater from the springs and in boreholes was from mantle origin, and it can be very likely attributed to the degassing of the mantle in the neighboring Eifel volcanic fields, located at a distance less than 100 km eastward. The role of the deep-rooted fractures that act as CO_2 transport pathway to the surface are still to be clarified, but several major thrust faults exist in the Rhenish Massif and could have connected the Eifel area with the studied area.

Code availability. No specific code was used for this publication. All data and equations were implemented in Microsoft Excel.

Data availability. All the data that made it possible to draw the conclusions of this article are presented in Table 1. The company's internal hydrochemical analysis data on mineral waters cannot be shown for reasons of confidentiality. When data from other publications are used, they are accessible in the publication mentioned and included in Table 1.

Author contributions. AD is the main contributor of this paper and worked on the conceptualization, the methodology, the field investigation, the writing of the paper and the visualization of the data. P-HB worked consequently on the validation of the methodology and data, the field investigation, the writing, editing and proof reading of the work, and the funding acquisition. LZ was in charge of the noble gas analysis. PJ, AC and FN supervised the work and helped with access to internal data for wells and springs where samples were taken. AD is the main supervisor of the work and consequently also worked on the project administration, paper proofreading and editing, and funding acquisition.

Competing interests. The contact author has declared that neither they nor their co-authors have any competing interests.

Disclaimer. Publisher's note: Copernicus Publications remains neutral with regard to jurisdictional claims in published maps and institutional affiliations.

Acknowledgements. This work is part of the ROSEAU project, as part of the Walloon program "Doctorat en Entreprise", co-funded by the SPW Région Wallonne of Belgium and the company Bru-Chevron S.A. (Spadel S.A.), under grant number 7984. The collaboration with the CRPG of Nancy was made possible thanks to the Europlanet Transnational Access Program, as this project has received funding from the European Union's Horizon 2020 research and innovation program under grant agreement no. 871149. The authors acknowledge these two institutions for their support.

Financial support. This research has been supported by the Service Public de Wallonie (grant no. 7984) and the Horizon 2020 (EPN-2024-RI (grant no. 871149)).

Review statement. This paper was edited by Brian Berkowitz and reviewed by two anonymous referees.

References

Aeschbach-Hertig, W., Kipfer, R., Hofer, M., Imboden, D., Wieler, R., and Signer, P.: Quantifiction of gas fluxes from sub-

continental mantle: the example of Laacher See, a maar lake in Germany, Geochim. Cosmochim. A., 60, 31–41, https://doi.org/10.1016/0016-7037(95)00370-3, 1996.

Agnew, R. J.: Why springs bubble: A framework for gas discharge in groundwater, Groundwater, 56, 859–870, https://doi.org/10.1111/gwat.12789, 2018.

Andrews, J. and Kay, R.: Natural production of tritium in permable rocks, Nature, 298, 361–363, https://doi.org/10.1038/298361a0, 1982.

Barros, R., Defourny, A., Collignon, A., Jobé, P., Dassargues, A., Piessens, K., and Welkenhuysen, K.: A review of the geology and origin of CO_2 in mineral water springs in east Belgium, Geol. Belg., 24, 17–31, https://doi.org/10.20341/gb.2020.023, 2021.

Barry, P. H., Negrete-Aranda, R., Spelz, R. M., Seltzer, A. M., Bekaert, D. V., Virrueta, C., and Kulongoski, J. T.: Volatile sources, sinks and pathways: A helium-carbon isotope study of Baja California fluids and gases, Chem. Geol., 550, 119722, https://doi.org/10.1016/j.chemgeo.2020.119722, 2020.

Bekaert, D., Broadley, M., Caracausi, A., and Marty, B.: Novel insights into the degassing history of the Earth's mantle from high precision noble gas analysis of magmatic gas, Earth Planet. Sci. Lett., 525, 115766, https://doi.org/10.1016/j.epsl.2019.115766, 2019.

Bräur, K., Kämpf, H., Niedermann, S., and Strauch, G.: Indications for the existence of different magmatic reservoirs beneath the Eifel area (Germany): A multi-isotope (C,N,He,Ne,Ar) approach, Chem. Geol., 56, 193–208, https://doi.org/10.1016/j.chemgeo.2013.08.013, 2013.

Carreira, P., Marques, J., Carvalho, M., Nunes, D., and da Silva, M. A.: Carbon isotopes and geochemical processes in CO_2-rich cold mineral water, N_Portugal, Environ. Earth Sci., 71, 2941–2953, 2014.

Depret, M., Bruni, Y., Dassargues, A., Defourny, A., Marion, J.-M., Vanderschueren, W., and Hatert, F.: Mineralogical and hydrogeological study of "pouhons" in the lower Paleozoic formations of the Stavelot-Venn Massif, Geologica Belg., 24, 109–124, 2021.

Dunai, T. and Baur, H.: Helium, neon, and argon systematics of the European subcontinental mantle: Implications for its geochemical evolution, Chechim. Cosmochim. A., 59, 2767–2783, https://doi.org/10.1016/0016-7037(95)00172-V, 1995.

Fielitz, W. and Mansy, J.-L.: Pre- and synorogenic burial metamorphism in the Ardenne and nieghbouring areas (Rhenohercynian zone, central European Variscides, Tectonophysics, 309, 227–256, https://doi.org/10.1016/S0040-1951(99)00141-9, 1999.

Fillimonova, E., Lavrushin, V., Kharitonova, N., Sartykov, A., Maximova, E., Baranovskaya, E., Korzun, A., Maslov, A., and Baidariko, E.: Hydrogeology and hydrochemistry of mineral sparkling groundwater within Essentuki area (Caucasian mineral water region), Environ. Earth Sci., 79, 15, https://doi.org/10.1007/s12665-019-8721-2, 2020.

Gilfillan, S., Györe, D., Flude, S., Johnson, G., Bond, C., Hicks, N., Lister, R., jones, D., Kremer, Y., Haszeldine, R., and Stuart, F.: Noble gases confirm plume-related mantle degassing beneath Southern Africa, Nat. Commun., 10, 5028, https://doi.org/10.1038/s41467-019-12944-6, 2019.

Goes, S., Spakman, W., and Bijwaard, H.: A lower mantle source for central European volcanism, Science, 286, 1928–1931, 1999.

Graham, D. W.: Noble gas isotope geochemistry of mid-ocean ridge and ocean island basalts: Characterization of mantle source reservoirs, 2002.

Holocher, J., Matta, V., Aeschbach-Hertig, W., Beyerle, U., and Hofer, M.: Noble gas and major element constraints on the water dynamics in an alpine floodplain, Groundwater, 39, 841–852, 2001.

Vanderschueren, H. W.: Le radon dans l'air, dans l'eau et dans les roches. Mesure dynamique de son exhalation et contribution á la charactérisation géologique des matériaux, Geological survey of Belgium professional paper, 308, 96 pp., http://biblio.naturalsciences.be/rbins-publications/professional-papers-of-the-geological-survey-of-belgium/bibliographic-references/vanderschueren_radon_2011 (last access: 18 May 2022), 2011.

Karolyte, R., Johnson, G., Györe, D., Serno, S., Flude, S., Stuart, F., Chivas, A., Boyce, A., and Gilfillan, S.: Tracing the migration of mantle CO_2 in gas fields and mineral water springs in south-east Australia using noble gas and stable isotopes, Geochim. Cosmochim. A., 259, 109–128, https://doi.org/10.1016/J.gca.2019.06.002, 2019.

Kreemer, C., Blewitt, G., and Davis, P. M.: Geodetic evidence for a buoyant mantle plume beneath the Eifel volcanic area, NW Europe, Geophys. J. Int., 222, 1316–1322, https://doi.org/10.1093/gji/ggaa227, 2020.

Marty, B., Almayrac, M., Barry, P., Bekaert, D., Broadley, M., Byrne, D., Ballentine, C., and Caracausi, A.: An evaluation of the C / N ratio of the mantle from natural CO_2-rich gas analysis : Geochemical and cosmochemical implications, Earth Planet. Sci. Lett., 551, 116574, https://doi.org/10.1016/J.epsl.2020.116574, 2020.

May, F., Hoernes, S., and Neugebauer, H.: Genesis and sitribution of mineral waters as a consequence of recent lithospheric dynamics: the Rhenish Massif, Central Europe, Geol. Rundsch., 85, 782–799, https://doi.org/10.1007/s005310050112, 1996.

Moreira, M., Rouchon, V., Muller, E., and Noirez, S.: The xenon isotopic signature of the mantle beneath Massif Central, Gechem. Perspect., 6, 28–32, 2018.

Pisolkar, M.: Why CO_2-rich mineral waters present peculiar signatures, when compared with other types of mineral waters? Vidago-Pedras Salgadas case study, Master Thesis, Tecnico Lisboa, Lisboa, Portugal, https://fenix.tecnico.ulisboa.pt/downloadFile/1689244997257994/dissertacao.pdf (last access: 9 May 2022), 2017.

Ray, J. S.: Carbon isotopic variations in fluid-deposited graphite: evidence for multicomponent Rayleigh isotopic fractionation, Int. Geol. Rev., 51, 45–57, https://doi.org/10.1080/00206810802625057, 2009.

Redondo, R. and Yelamos, J. G.: Determination of CO_2 origin (natural or industrial) in sparkling bottled waters by $^{13}C/^{12}C$ isotope ratio analysis, Food Chem., 92, 507–514, 2004.

Ritter, J., Jordan, M., Christensen, U., and Achauer, U.: A mantle plume below the Eifel volcanic fields, Germany, Earth Planet. Sci. Lett., 186, 7–14, https://doi.org/10.1016/S0012-821X(01)00226-6, 2001.

Sano, Y. and Fischer, T.: The analysis and interpretation of noble gases in modern hydrothermal systems, in: The Noble Gases as Geochemical Tracers, edited by: Burnard, P., 249–317, Springer, https://doi.org/10.1007/978-3-642-28836-4_10, 2013.

Sano, Y. and Marty, B.: Origin of carbon in fumarolic gas from island arcs, Chem. Geol., 119, 265–274, 1995.

Stiller, M., Kaerger, L., Agafonova, T., Krawczyk, C., Oncken, O., Weber, M., Former DEKORP Project Leaders, Former DEKORP/BELCORP Research Group, Former DEKORP Processing Centre: Deep seismic reflection profile DEKORP 1987-1A across the western Rhenish Massif, West Germany/ East Belgium, GFZ Data Services, https://doi.org/10.5880/GFZ.DEKORP-1A.001, 2020.

Vanbrabant, Y., Braun, J., and Jongmans, D.: Models of passive margin inversion: implications for the Rhenohercynian fold-and-thurst belt, Belgium and Germany, Earth Planet. Sci. Lett., 202, 15–29, https://doi.org/10.1016/S0012-821X(02)00751-3, 2002.

Zimmermann, L. and Bekaert, D.: Analyse des gaz rares par spectrométrie de masse statique – Mesures et applications.J6637 V1(Techniques de l'ingénieur), 2020.

Zimmermann, L., Füri, E., and Burnard, P.: Purification des gaz rares sous ultravide – Méthodes de purification. Techniques de l'Ingénieur, J6 635, 2015.